ORIENTAL JOURNAL OF CHEMISTRY
An International Open Access, Peer Reviewed Research Journal
www.orientjchem.org
ISSN: 0970-020 X
CODEN: OJCHEG
2025, Vol. 41, No.(1):
Pg. 11-24

Development and Optimization of Roflumilast-loaded Nanostructured Lipid Carrier (NLCs) Formulation for Topical Delivery

ABHISHEK SINGH[1]*, PRASHANT KUMAR[2] and ANURAG VERMA[1]

[1]Department of Pharmaceutics, Teerthanker Mahaveer College of Pharmacy, Teerthanker Mahaveer University, Moradabad (UP)-244001, India.
[2]Department of Pharmaceutics SRM Modinagar College of Pharmacy, SRMIST Delhi-NCR Campus, Modi Nagar, Ghaziabad Uttar Pradesh-201204, India.
*Corresponding author E-mail: abhishek0794@gmail com

http://dx.doi.org/10.13005/ojc/410102

(Received: December 21, 2024; Accepted: February 17, 2025)

ABSTRACT

The development of innovative drug delivery methods is essential to getting past the drawbacks of present pharmacological regimens, including fast metabolism, high toxicity, low solubility, and fluctuations in plasma drug levels. With fewer side effects and improved medication solubility, stability, bioavailability, and targeted delivery, nanostructured lipid carriers (NLCs) offer a viable alternative. The creation and improvement of Roflumilast-loaded NLCs, a phosphodiesterase-4 (PDE-4) inhibitor used to treat psoriasis, is the main topic of this work. A two-factor, three-level experimental design and Design Expert® software were used for creating eight formulation batches with varying quantities of oleic acid, Tween 80, and glyceryl monostearate (GMS). UV-spectrophotometry, NMR, FTIR, DSC, XRD, particle size measurement, transmission electron microscopy (TEM), %entrapment efficiency (%EE), and *in-vitro* cumulative drug release (%CDR) were among the methods used to characterize the NLCs. With a particle size of 122.65nm, the polydispersity index (PDI) was 0.278 and the zeta potential of –20.16 mV, the optimized formulation (F3) demonstrated exceptional stability and uniformity. While FTIR and DSC analyses showed that Roflumilast and the excipients were compatible without causing significant chemical interactions, TEM investigation verified the spherical morphology and absence of aggregation. F3 had %EE and %CDR of 87.76% and 88.29%, respectively, demonstrating the effective drug encapsulation and release characteristics of the NLCs. XRD analysis verified that the medication was crystalline inside the lipid matrix. All things considered, the created Roflumilast-loaded NLCs show great promise for better medication delivery in dermatological applications, providing increased therapeutic efficacy and stability.

Keywords: Nanostructured lipid carriers, Roflumilast, Drug delivery, Phosphodiesterase-4 inhibitor, Optimization, Encapsulation efficiency, Bioavailability.

INTRODUCTION

Nowadays it has become clear the creation of innovative drug delivery methods is not enough to ensure advancements in drug therapy. Disappointing outcomes in the *in vivo* or clinical setting frequently trail intriguing *in vitro* experimental data. The main causes of this failure are the drug's rapid metabolism, which results in insufficient drug concentration in the body; its widespread distribution, which causes high drug toxicity; its poor solubility in formulations; and the great variability or variation of plasma drug levels among subjects[1]. Creating workable medicine delivery devices is a promising first step toward solving this issue. Several approaches have been investigated in recent decades to create drug-carrier systems that are nanoscale. Drug delivery devices known as nanostructured lipid carriers (NLCs) employ a core matrix collected of fluid and hard lipids. Compared to conventional carriers, NLCs provide several benefits for medication therapy, such as enhanced solubility, increased permeable properties and Bioavailability side effects, extended ½ lifespan, and tissue-targeted dosing, Lately, NLCs have garnered a growing amount of interest[2]. NLCs' occlusive properties can increase skin moisture and aid in medication absorption. Furthermore, the lipids and surfactants that makeup NLCs can function as permeability enhancers to facilitate the thinning or fluidization of the stratum corneum's lipid bilayers (SC)[3]. Oxidative stress (OS) is frequently caused by environmental insults to the skin that occur in modern living, such as increased air pollution and excessive sun exposure. These circumstances can lead to Reactivity of oxygen species (ROS) overproduction, which can overwhelm the skin's deteriorating capacity and cause skin problems[4]. Psoriasis is a known autoimmune skin disease that causes inflammation and affects 2-3% of people globally. Psoriatic arthritis and psoriasis are both relapsing and remitting conditions[5,6]. Roxadustat is a chemical roflumilast. It appears as a powder that ranges from white to off-white. With a chemical formula of $C_{17}H_{14}Cl_2F_2N_2O_3$, (Fig. 1) & the mass of the molecule is 403.21 $gmol^{-1}$, it is easily dissolved in acetone, slightly soluble in ethanol, and almost insoluble in H_2O, C_7H_{16}, & C_6H_{14}.

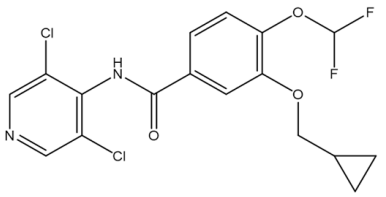

Fig. 1. Structure of Roflumilast

PDE-4 (phosphodiesterase 4) inhibitor roflumilast has been used to treat psoriasis. Phosphodiesterase-4 controls the amount of cAMP inside cells. Worldwide, rofumilast, a selective PDE-4 inhibitor medication, is now available for psoriasis sufferers. The enzyme phosphodiesterase type 4 (PDE-4) participates in the maintenance of intracellular cyclic adenosine monophosphate (cAMP) levels[7] and the biological responses of several cell types, including immune cells, to external stimuli[8]. PDE-4 activity is greater in psoriatic skin compared to normal skin[9], & immune modulators like growth mortification factor α, ILs-γ, ILs-17, & ILs-23 are down-regulated when PDE-4 is inhibited[10]. Aprecimilast, an oral PDE-4 inhibitor, is authorized to treat moderate-to-severe plaque psoriasis[11] and crisaborole ointment has been approved for the treatment of atopic dermatitis[12,13]. A key function in tissue inflammation has been found for each of the four subfamilies of PDE4 (A, B, C, and D). Immunologic cells such as dendritic cells, T cells, macrophages, and monocytes exhibit significant expression of PDE4. Immune cells produce fewer proinflammatory mediators and more of the anti-inflammatory cytokine IL-10 when cAMP induces a downregulatory signal in them. As a result, PDE4 inhibition raises cAMP levels, which in turn inhibits the NF-kB pathway. This reduces nearly every cytokines that is pro-inflammatory, namely TNF-a, IL-1, IL-8, IL-12, IL-23, and CCL20, in all inflammatory cells. Certain anti-inflammatory PDE4 inhibitors are being evaluated as dermatological therapies, especially for psoriasis.

MATERIALS AND METHODS

Materials

Roflumilast was obtained from Zydus Life Science Ltd, Sanand, Ahmedabad, India, and Glycerol monostearate, oleic acid, tween 80, were available in the Central store of Teerthanker Mahaveer College of Pharmacy, TMU. Every other chemical and solvent utilized in the research was of the caliber of an analytical reagent.

Methods

Ultraviolet (UV) spectrophotometer

Preparation of standard solution

To establish a primary stock solution, 100 mg of roflumilast was carefully weighed into 100 mL of a volumetric flask and dissolved in methanol to a level of 1000 µg/mL. Use methanol to further dilute One ml of the main stock solution to ten ml to achieve the necessary concentration of 100 µg/mL. Use methanol to dilute 0.2 mL of secondary stock solution to 10 mL to achieve the necessary concentration of 2 µg/mL[14].

Selection of wavelength for analysis of Roflumilast Measured precisely to achieve a concentration of 2 µg/mL, A 10 mL volumetric container was filled with 0.2 mL of 2 stock, which was then diluted to 10 mL. The maximum wavelength was detected by a first spectral scan in the 200-400 nm range, and additional dilutions for linearity were made from the stock solution using the usual approach. The wavelength range of 248-250 nm was found to be the greatest. then Get a calibration plot ready[14].

Nuclear magnetic resonance (NMR)

Samples were made by dissolving them in DMSO, adding tetramethyl saline (TMS) as an internal standard, and then radioactively irradiating them. A graph showing the amount of energy absorbed in opposition to a strong magnetic field is the NMR spectrum wave[15].

Fourier-transform infrared spectroscopy (FTIR)

The Fourier transform infrared spectrophotometer instrument (Make: Perkins Elmer, the United States; Model: Frontier Optica with spectrum software) was used to analyze the Fourier transform infrared spectrum of drugs, single additives, and their physical combinations. Following the trituration of 5 mg of the sample and 500 mg of the potassium bromide in a mortar, the mixture was crushed in a hydraulic press into a KBr disc. The disc was placed in a chamber filled with dry nitrogen. 32 scans on average were carried out with a wavelength resolution of 2 cm^{-1} to get the spectrum in the 400-4000 cm^{-1} region[16].

Differential scanning calorimetry (DSC)

Drugs, separate ingredients, and their physical mixtures of them subjected to DSC analysis using a DSC apparatus (Model: DSC 6000; manufactured in the United States by PerkinElmer). The melting points of zinc (419.7°C) and indium (156.6°C) were used to calibrate the device for temperature. A sample of 1-2 mg (ingredients and physical mixes) was measured right away using a Sartorius balance (Germany) and sealed in an aluminum pan. It was then tested in the ambient temperature of 30°C-340°C at a rate of heating of 10°C min^{-1} in a nitrogen atmosphere with an average flow rate of 20 mL/minute. Pyris software was used to analyze the collected DSC curves and look for any interactions[16].

X-ray diffraction (XRD) study

The X-ray diffraction coefficient $\theta/2\theta$ was determined utilizing a Siemens D-501 (Siemens, Germany) diffractometer (coupled $\theta/2\theta$) in the Bragg-Brentano pattern. A secondary graphite monochromator was employed in conjunction with CuKα radiation[17].

Formulation development

Preparation of NLCs as per the Experimental Design

Design Expert® (Version 12.0.3.0). The response surface model was illustrated using software that obtained the combination of variables. To optimize the NLC synthesis technique, a two-, two-level three-factor experimental design was used. Utilizing Designs Experts® (the latest version 12.0.3.0), investigate the response surfaces which were represented by an optimization process with a minimal number of experimental runs (in the present research vocation 08 runs). The independent factors selected were concentration of GMS (X1), Concentration of Oleic acid (X2), and amount of tween 80 (X3) with their set low (–1), and high (+1) levels; chosen based on first investigations. The dependent responses under investigation were the entrapment efficiency (Y2), particle size (Y1), and % Cumulative drug release (Y3). Three factors and just eight runs are required, thereby indicating Both time and energy usage are reduced. Every element is also examined and classified at three fundamental levels. An outline of the implied dependent and independent variables is presented in Table 1.

Table 1: 2^3 Response variables and full-factorial design of roflumilast-loaded NLCs (n=3)

Formulation Code,	Coded rate X1	Actual rate X1	C value X2	Actual value X2	C rate X3	Actual rate X3
F_1,	1	200	-1	0.3	1	2%
F_2,	1	200	1	0.6	-1	1%
F_3,	-1	100	1	0.6	-1	1%
F_4,	-1	100	1	0.6	1	2%
F_5,	-1	100	-1	0.3	-1	1%
F_6,	1	200	-1	0.3	-1	1%
F_7,	1	200	1	0.6	1	2%
F_8,	-1	100	-1	0.3	1	2%

(X1 =GMS, X2= Oleic acid, X3= Tween 80)

Preparation of NLC

Applying high-pressure homogenization, NLC formulations including roflumilast were created. A liquid lipid, solid lipid, and measured roflumilast were precisely melted at 70±2°C while being continuously stirred, producing a transparent mixture. Separately, the aqueous phase was created by dissolving tween-80 in water at 100°C and keeping the temperature at 70±2°C. Using a high-speed homogenizer that was continuously agitated at 2000 rpm, the aqueous phase was gradually introduced to the lipid phase. After that, this combination went through a high-pressure homogenizer. (Unigenetics Instruments Pvt. Ltd, India) at 20,000 rpm to form NLCs. Subsequently, the resulting NLC dispersion was allowed to cool for ten minutes while being gently agitated[18].

The characteristics of nlcs

Zeta potential and particle size of NLCs

The diameter of the particles was measured using the dynamical light scattering method at 25 ± 1°C and 90° temperatures and scattered angle, respectively, using a Zeta-sizer from Malvern Instrumentation Ltd., UK. The zeta potential at 25°C was measured using the same apparatus. Three tests were conducted on it[19].

Morphology of NLCs

On a 400-network carbon-coated copper disc, a single drop of NLCs was applied, and the extra liquid was wiped off using tissue paper. To the framework, A 2% w/v solution of neutralized phosphotungstic acid was introduced as a drop. Before being examined at 4000 X, the Samples that had been dyed were left to air dry at the ambient temperature. TEM pictures were obtained using a 200 kV accelerating voltage[20].

Entrapment efficiency (%EE)

The entrapment efficiency of roflumilast NLCs was evaluated indirectly by determining the quantity of free roflumilast in the dispersed aqueous phase. In conclusion, cooling centrifugation (REMI Instruments Ltd., India) was used to centrifuge two milliliters of the roflumilast NLCs dispersion in an Eppendorf tube for 20 min at 12,000 rpm (4°C). After a sufficient dilution with methanol[21], the supernatant was filtered, and the quantity of roflumilast was measured by UV-spectroscopy at 248 nm. The following formula was used to get the rate of entrapment%.

$$EE(\%) = \frac{(\text{The total amount of roflumilat}) - (\text{Quantity of free roflumilast in supernatant}) \times 100}{\text{Total quantity of roflumilast}}$$

***In vitro* drug release studies**

The drug release profile of Roflumilast-NLCs was measured for 24 h at skin temperature and pH using Franz diffusion cells. A 2.4 nm-pore-sized, semi-permeable cellulose membrane (MW 12,000-14,000 Da) was attached between the donor and receptor compartments after being soaked in (PBS, pH 7.4) for the entire night. The releasing membrane's surface area measured 3.14 cm^2. PBS was added to the receptor compartment, which was kept at 37±0.5°C, & swirled at 700 rpm using a magnetic stirrer. The donor section was occupied with 1 milliliter of Roflumilast-NLCs, which contained 0.5 milligrams of Roflumilast. Methanol was utilized as a co-solvent to keep the sink conditions constant during the investigation because it has been discovered that the Roflumilast in PBS varies less. Aliquots (3 mL) were taken out of the receptor compartment at regular intervals (15, 30, 45, 60 min and 2, 4, 8, 12, 24 hours). An equivalent volume of PBS was added right away to replace the volume that was removed. The UV-Visible spectrophotometer (UV-

1900i, Shimadzu) at 248 nm was used to measure the concentration of the medication emitted at various time intervals[22].

RESULT AND DISCUSSION

Pre-formulation studies

UV Spectrophotometer

Absorption maxima (λ_{max}) of the roflumilast conducted in methanol was found to be 248 and depicted in Figure 1.

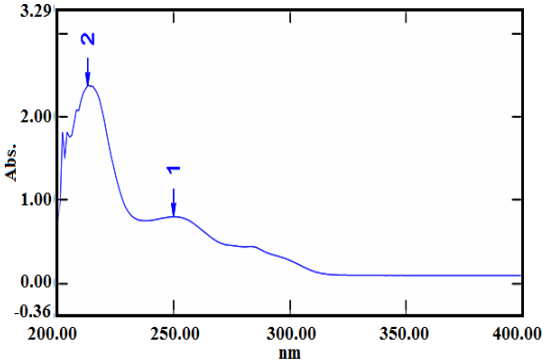

Fig. 2. UV-spectrophotometer of roflumilast

NMR

In NMR spectra at 7-8 ppm shows 5 signals that show the aromatic protons and at 4 ppm shows 1 signal of proton of CH2 at mid of oxygen and cyclopropane and 1.6 ppm one signal shows for 1 proton of NH in the aromatic ring and also 0-1.5ppm that shows 3 signal of proton of cyclopropane and all others that shows in structure of the drug. The data are shown in Figure 2.

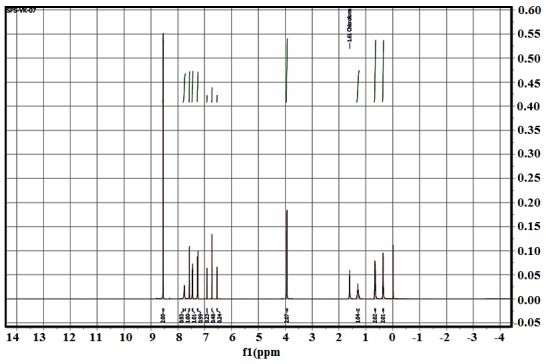

Fig. 3. NMR spectra of roflumilast

FTIR Study

Roflumilast, Glyceryl Monostearate, Oleic Acid and Tween 80 molecular structure exhibits several peaks, such as O-H or N-H elongating (3200-3500 cm^{-1}), C-H elongating (2800-3000 cm^{-1}), C=O (carbonyl) elongating (1700-1750 cm^{-1}), C=C elongating (1600-1500 cm^{-1}), C-O stretching (1000-1300 cm^{-1}), (Figure 3).

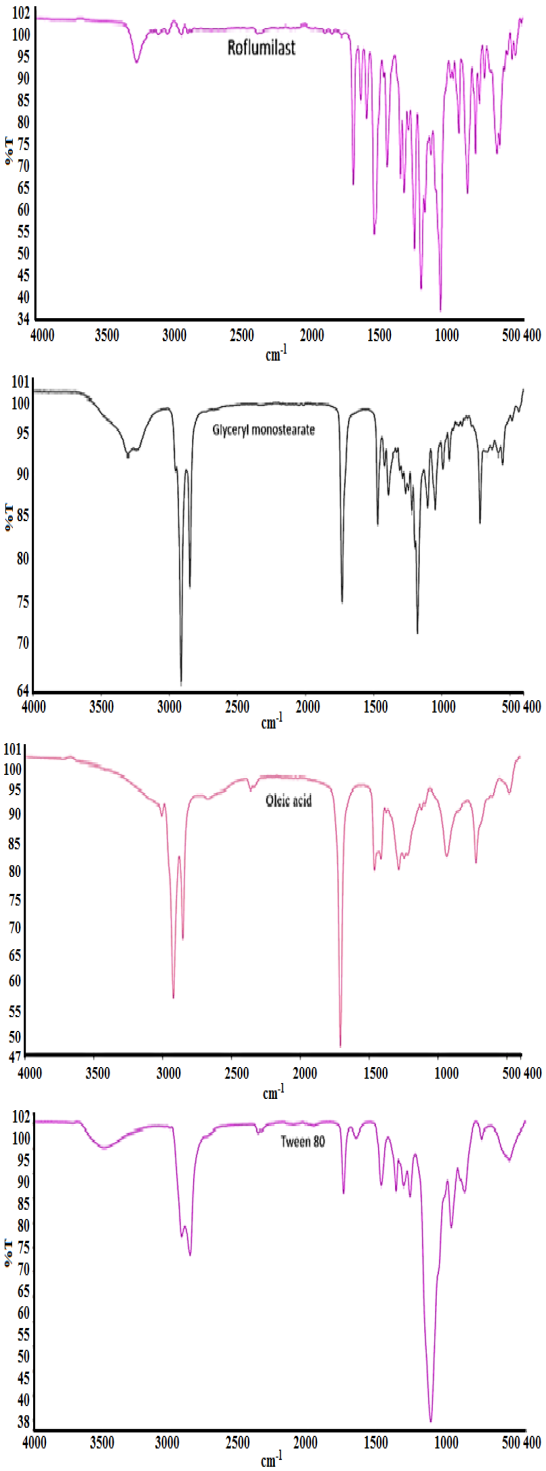

Fig. 4. FT-IR spectra of RFL and excipients: Glyceryl Monostearate (GMS), Oleic acid (OA), Teen 80 (T80)

The presence of peaks in the above regions confirms the structural components of Roflumilast, such as amide (N-H), ester (C=O), and aromatic C=C bonds. The exact locations and intensities of these peaks help in the identification and confirmation of the drug. Glyceryl monostearate, being a fatty acid ester, shows characteristic peaks for both C-H elongating from the long alkyl chain and C=O stretching from the ester group. This confirms its identity as a lipid component. Oleic acid, being a fatty acid, shows the expected peaks for the C-H elongating of the alkyl chain and the sharp peak for the carboxyl C=O bond. This confirms the presence of oleic acid as a fatty acid component. Tween 80, a surfactant, shows characteristic peaks for ester C=O stretching and C-H stretching from its long alkyl chains. The presence of ether and ester groups is confirmed by the strong absorption in the 1100-1300 cm^{-1} region[23].

Compatibility study of drug and polymer

Roflumilast, with several excipients exhibits several peaks, such as O-H or N-H elongating (3200-3500 cm^{-1}), C-H elongating (2800-3000 cm^{-1}), C=O (carbonyl) elongating (1700-1750 cm^{-1}), C=C stretching (1600-1500 cm^{-1}), C-O stretching (1000-1300 cm^{-1}), shown in Figure 4.

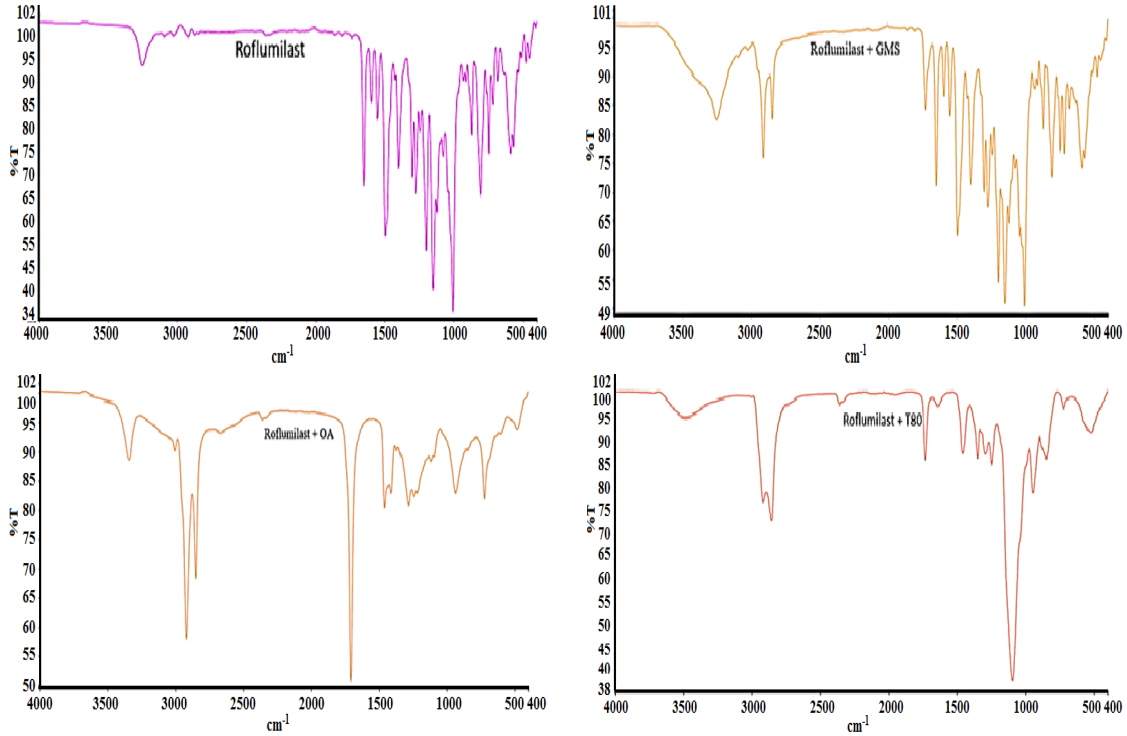

Fig. 5. Roflumilast along with its 1:1 (w/w) physical mixes' FT-IR spectrum

With no significant peak changes or disappearances, the spectrum reveals a combination of Roflumilast and GMS peaks, suggesting that there is probably little to no chemical interaction between the two components. The medication and excipient's respective distinctive peaks are still discernible in the physical mixture, indicating compatibility. Roflumilast and oleic acid together exhibit additive spectrum characteristics from both substances. Both the C-H elongating from the alkyl chain and the C=O elongating from oleic acid and roflumilast indicate that there isn't much of a chemical interaction between the two, proving that the physical mixture is compatible. The combination of Roflumilast and Tween 80 exhibits the distinctive peaks of each component, much like the other mixes. Key peaks do not significantly change or disappear, indicating a weak chemical interaction between the two and corroborating their physical compatibility. Finally, the spectra indicate that roflumilast is safe to use with Tween 80, oleic acid, and glyceryl monostearate. Since Roflumilast's main peaks remain consistent throughout the mixes, it appears that the excipients do not affect the drug's chemical structure[24].

DSC

The initial thermogram reveals a sharp

peak in endothermic activity at 160-170°C, which most likely correlates to Roflumilast's melting point. This is typical for crystalline substances, indicating a phase transition from solid to liquid. After the melting peak, there appears to be a broad endothermic event starting near 350°C, suggesting possible thermal degradation or decomposition. The stable region after the melting peak indicates some thermal stability up to a higher temperature. The second thermogram shows a broad endothermic peak around 50-75°C, which resembles to the melting point of Glyceryl monostearate. Broadness of the peak suggests that Glyceryl monostearate is a more complex compound, likely exhibiting polymorphic behavior or existing in multiple forms (alpha, beta) shown in Figure 5.

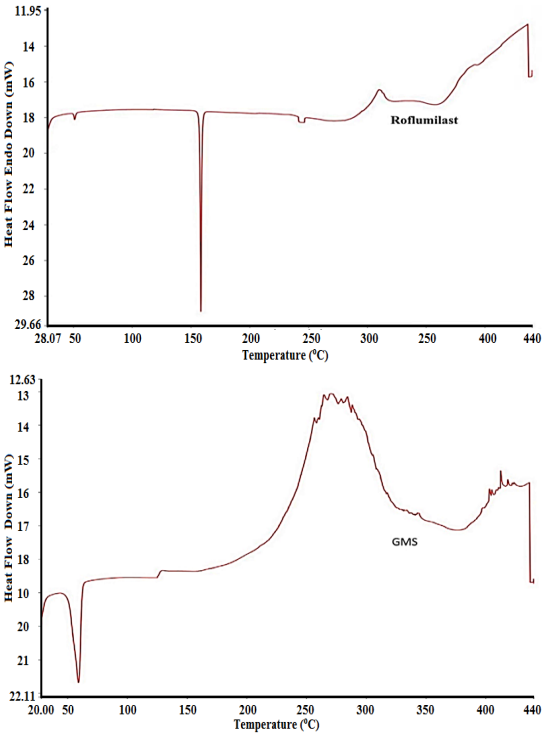

Fig. 6. DSC curves of RFL and GMS

The sharp melting point at 160-170°C and subsequent stability suggest that it is a relatively pure crystalline compound with a distinct melting point, followed by thermal degradation around 350°C. The broad, lower temperature melting peak suggests it has a more complex structure or multiple forms. Its thermal behavior suggests that it might undergo polymorphic transitions before reaching the decomposition phase at higher temperatures. The difference in the thermal behavior of these two substances can be attributed to their chemical nature: Roflumilast is a well-defined crystalline drug, while Glyceryl monostearate is an excipient that can exist in multiple crystalline forms. This can be important for formulation development when both materials are used in combination, as thermal stability and interactions between them can affect the overall stability of the product shown in Figure 6[25].

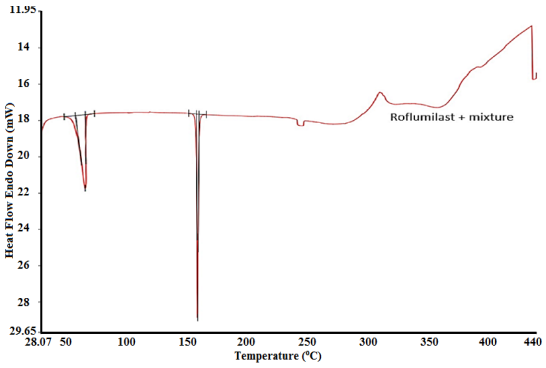

Fig. 7. DSC curves of RFL and mixture

A physical mixture including Roflumilast and another material (perhaps an excipient like Glyceryl monostearate from the preceding image) is represented by the thermogram (Roflumilast+ Mixture). There is a sharp endothermic peak at about 160–170°C, which indicates that Roflumilast is present in the combination. This implies that there is no discernible change in Roflumilast's melting point in the mixture. Other minor peaks can indicate melting or phase changes of the excipient in the vicinity of 50–100°C. The previous thermogram indicates that components like Glyceryl monostearate, or a comparable chemical, have a lower melting point, which is likely the reason of this[26].

XRD

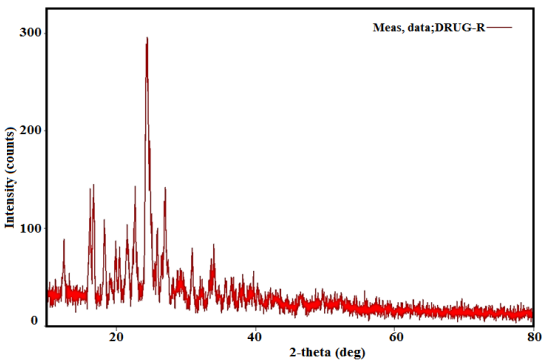

Fig. 8. XRD of roflumilast

The XRD θ/2θ scans as might be expected from a crystalline material, the spectrum derived from roflumilast powder shows low, flat background diffraction peaks that are rather clear and identifiable. The determined crystal structure and the diffraction pattern accord well. Conversely, there are no signs of the crystalline Roflumilast phase. More accurate measurements were made at specific diffraction angles to consistently rule out the occurrence of the original crystal construction as an applicable phase because the low segment of roflumilast in the ternary mixture is near the finding limit of the data that were provided shown in Figure 7.

Formulation development

Experimental Design for the Formulation of NLCs

A collection of numerical techniques known as response surface methodology (RSM) aids in the methodical examination of the formulations. The method makes it possible to optimize the crucial process variables that have an impact on the response surface. RSM allows for the quantification of the relationship between process parameters at various levels using the response surfaces that are created. Design Expert® (Version 12.0.3.0) was used To assess primary nonlinear effects & the relationship between independent and dependent factors in the primary composite quantitative screening design. The central composite design is one of the response surface designs that has many advantages over other designs. It also includes a multidimensional cube's duplicate center point. As a result, only three levels of factors need to be tested, and severe treatment combinations are also avoided. Furthermore, the distance from the design center point is the only factor that affects the variation of the expected response at any given location. Low, medium, and high levels correspond to the coded and real values of the dependent and independent variables of the applicable CCD. Eight distinct NLC formulation batches have been produced as a result of the factor combinations based on experimental design[27]. Different NLC batches were made and subsequently assessed for both responses by the recommendation. The observed responses were fitted to eight runs, and the quadratic equation for both dependent variables was found to be the best fit. The model's importance and the terms it generates and analysesd[28]. Table 2 displays all of the responses for the eight runs as well as the relationship between the independent and dependent variables.

Polynomial Equation

$$Y1=155.67-26.64X1+16.02X2+1.03X3-12.03\,X1X2+4.19X1X3+4.19X2X3-1.37X1X2X3 \quad (1)$$

According to polynomial Eq. 1, Y1 denotes Particle size while X1 is a concentration of GMS, X2 is a concentration of oleic acid and X3 is a concentration of tween 80. As per Eq. 1, GMS has a negative coefficient, indicating that increasing GMS concentration tends to decrease particle size. This suggests that GMS may aid in stabilizing smaller particles, Oleic Acid has a positive coefficient, meaning that higher concentrations of oleic acid are associated with an increase in particle size and Tween 80 shows a slight positive effect on particle size. However, the effect is minimal compared to GMS and Oleic Acid.

$$Y2=72.54+10.56X1+1.89X2-0.4625X32.29X1X2+0.5550X1X3+0.2375X2X3+3.92X1X2X3 \quad (2)$$

According to polynomial Eq. 2 all given %EE enhancers i.e. GMS, oleic acid, and tween 80. The GMS likely plays a significant role in encapsulating the active ingredient, oleic Acid also has a positive effect on entrapment efficiency, though the impact is smaller compared to GMS and A negative coefficient suggests that increasing Tween 80 concentration slightly decreases entrapment efficiency.

$$Y3=70.20-11.52X1+1.89X2-1.96X3+2.85X1X2+1.70X1X33.20X2X3+0.675X1X2X3 \quad (3)$$

According to polynomial Eq. 3 all given %CDR enhancers i.e. GMS, oleic acid, and tween 80. The GMS plays a pivotal role in reducing %CDR, beneficial for sustained-release formulations, oleic acid increases %CDR, and tween 80 has a nuanced effect, slightly reducing %CDR.

Table 2: Analysis of Variance

Response	Sum of square	DF	Mean Square	F -value	P-value	R2-value	Adequate precision	Model
Particle Size	7739.73	3	2579.91	7.10	0.0443	0.8419	6.481	Significant
%EE	922.13	3	307.38	7.33	0.0417	0.8469	5.657	Significant
%CDR	1120.92	3	373.64	8.62	0.0321	0.8660	6.603	Significant

Impact of independent variables on Particle size

The study reveals that X1 (GMS) and X2 (Oleic Acid) significantly influence particle size, with a decrease in size as oleic acid increases and GMS decreases. X2 (Oleic Acid) and X3 (Tween 80) also influence particle size, but their effect is less pronounced than in the X1X2 interaction. Higher concentrations of Tween 80 reduce particle size when oleic acid is kept lower. X1 (GMS) and X3 (Tween 80) show little impact on particle size when varied together, suggesting their interaction is not as critical as oleic acid's effect. The 3D surface plots provide valuable insights into how particle size is influenced by formulation components, especially oleic acid, Tween 80, and GMS. Oleic acid has the most substantial impact on particle size, especially when combined with GMS, as it is a surfactant that stabilizes particle sizes by reducing surface tension during the emulsification process[29]. Tween 80 also plays a role as a stabilizer, further reducing particle size when used in optimal concentrations. In summary, optimizing particle size reduction can be achieved by focusing on the interaction between oleic acid and GMS[30]. Tween 80 helps fine-tune particle size but plays a secondary role compared to oleic acid. Careful manipulation of oleic acid concentration is key, with GMS and Tween 80 serving as supplementary factors shown in Figure 8.

The Impact of Unrelated Factors on %Enchantment Efficiency

The study demonstrates the significant impact of GMS and Oleic Acid on encapsulation efficiency (%EE). GMS has a significant effect on %EE, with higher values indicating higher efficiency. Oleic Acid has a slight effect, suggesting that GMS concentration plays a serious role in improving %EE. The interaction among Oleic Acid & Tween 80 has minimal effect on %EE, suggesting their contribution might be marginal. GMS has a significant impact on %EE, with minimal variation across the range. Tween 80 shows minimal variation across the range, confirming that GMS is a critical factor in enhancing encapsulation efficiency. Surface plots show a strong gradient indicating a high dependency of %EE on GMS concentration. Oleic Acid and Tween 80 have a weaker influence on %EE[31]. GMS's surfactant properties help form stable NLCs systems, enhancing the drug encapsulation process. Tween 80's small effect may be due to its primarily solubilizing role, not significantly affecting the encapsulation process once GMS levels are optimized. Oleic Acid has a moderate effect but is not as pronounced as GMS. To maximize encapsulation efficiency, focusing on optimizing GMS concentration is the most effective strategy, with minor adjustments to Oleic Acid and Tween 80 concentrations as needed[32] shown in Figure 8.

Effect of independent variables on %CDR

The 3D plots of GMS and Oleic Acid show that both affect %CDR, with GMS being the dominant factor in regulating drug release. The interaction of GMS with Oleic Acid and Tween 80 demonstrates a strong dependency on GMS concentration, with increased GMS concentrations resulting in a higher cumulative drug release[33]. Oleic Acid and Tween 80 have a relatively moderate effect, with no significant impact on %CDR. The third Plot shows a strong influence of GMS on %CDR, with a clear upward slope as GMS increases. Tween 80's role is minimal, with no significant variation in cumulative drug release. The ability of GMS to enhance drug release could be attributed to its surfactant properties, which create stable NLCs for sustained drug release. The minor effect of Tween 80 could be due to its primary role as a solubilizer, which does not directly affect the drug release process in this formulation. Oleic Acid, acting as a stabilizer, does not significantly influence the release kinetics. In conclusion, to maximize cumulative drug release, GMS concentration should be carefully optimized, as it is the primary factor driving %CDR. Adjustments to Oleic Acid and Tween 80 concentrations would have minimal effect on drug release. Formulations aiming to enhance drug release should focus on GMS levels for effective results shown in Figure 8.

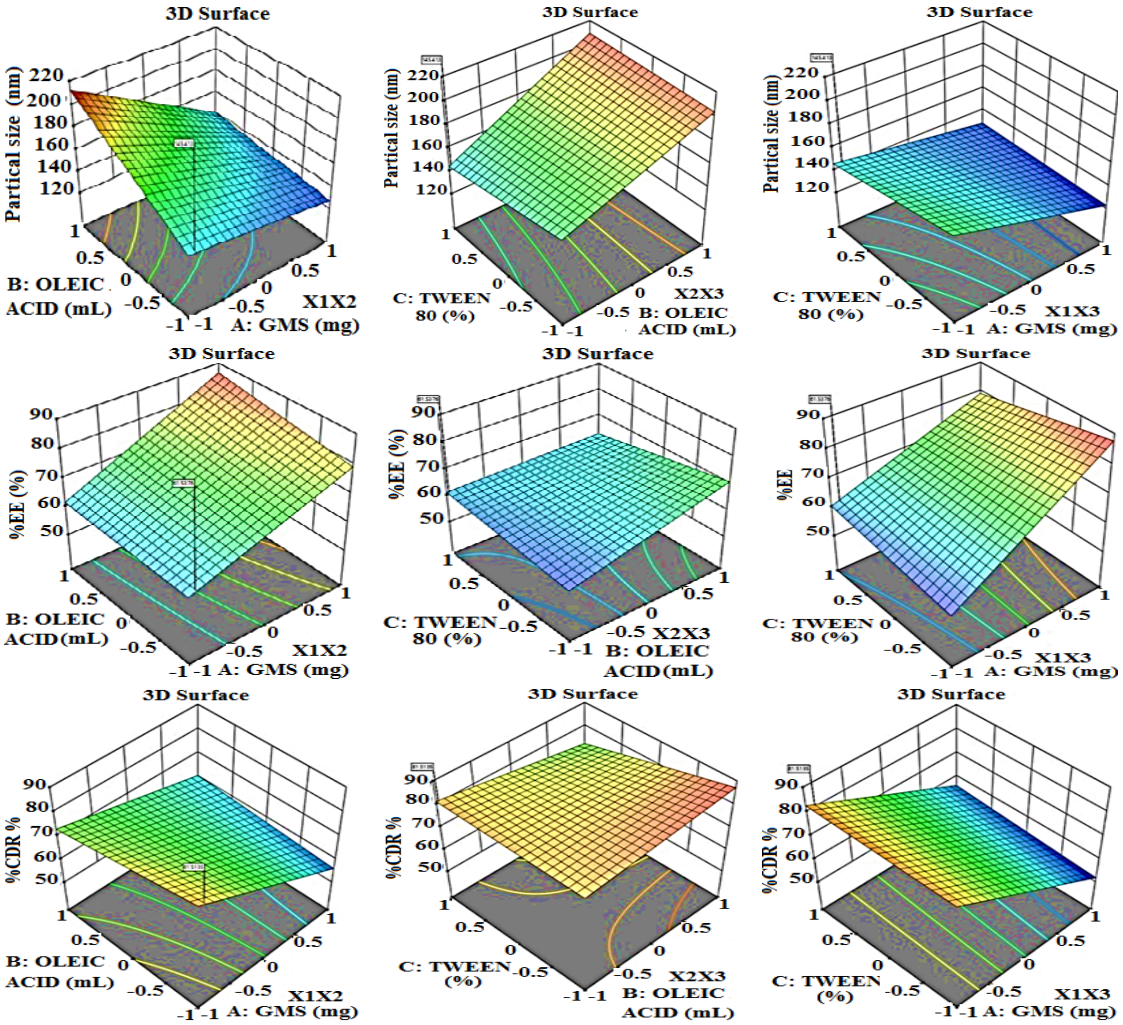

Fig. 9. Response 3D plots for the outcome of Conc. of GMS (X1), Conc. of Oleic acid (X2), & amount of tween 80 on Particle size, %EE & %CDR

Characterization of NLCs

PDI, Zeta potential, & Particle Size

It was found that the NLCs' PDI, zeta potential particle, & size ranged from 122.65 to 212.76 nm, 0.278 to 0.908, and -5.6 to -20.16 mV, respectively. The optimized formulation (F3) had particle size, zeta potential & PDI values of 122.65 nm, 0.278, and -20.16 mV, respectively. Table 3 displays the NLCs formulation's content as well as its particle size, PDI, and zeta potential. One of the key elements in determining the true impact of the active moiety is the dimension of the particle. The active component or smaller-sized nanoparticles typically have an easier time penetrating the skin's sheath & demonstrating their action. A further essential factor that affects the stability of the small particles is the zeta potential; the greater the zeta potential value, the more stable the lipidic nanoparticles will be because there will be less opportunity for them to aggregate as a result of electric repulsion between similar charges. The -vely particle has a stronger ability to pierce the skin[34-36].

Surface morphology

The TEM image displays many black areas, each of which represents a lipid nanoparticle. Differences in electron density are typically the cause of contrast in TEM pictures, with denser parts looking darker. The particles appear to be in the nanometre range, which is normal for NLCs based on the scale bar (500 nm). No notable aggregation is visible in the well-dispersed particle population. The majority of the particles are smaller than 200 nm, which is within the expected size range for NLCs, according to the

scale bar. Drugs encapsulated in smaller particles have improved stability and bioavailability, and they can pass through biological membranes more easily. The particles have a typical spherical form, which is characteristic of lipid nanoparticles. While there are some shape variations that could indicate a heterogeneous distribution in size, the particles are largely clearly defined. The spherical form of the particles helps to stabilize the NLCs over time by lowering surface energy. The homogeneous shape indicates a well-controlled formulation process, potentially utilizing methods such as ultrasonication or high-pressure homogenization shown in Figure 9.

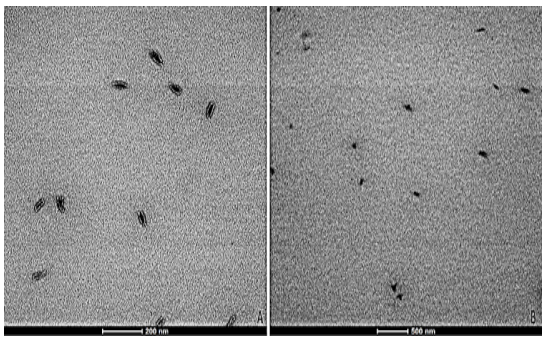

Fig. 10. TEM image of optimized formulation (roflumilast loaded NLCs

Entrapment efficiency

In the current study, It was found that the NLC formulations' encapsulation efficiency fell within the range of 54.92 to 87.76%. The %EE value of the optimized formulation (F3) was 88.28%, as shown in Table 3, indicating that it can hold more of the drug within its structure, Improving the delivery of drugs NLCs demonstrated their effectiveness as a carrier for weakly aqueously soluble or water-insoluble compounds. The addition of surfactants and other components to the formulation may help improve the drug's encapsulation within the NLC carrier[37].

In vitro drug release studies

The release study of the prepared formulations was determined by using a Franz diffusion cell. A total of eight formulations were prepared (F1 to F8) using polymers such as GMS, Oleic acid, and tween 80 in different concentrations. The results showed that the drug release of the prepared NLCs was in the range of 51.55% to 88.29% the formulation F3 is 88.29%, data shown in Table 3, indicating fast and efficient drug release[38], and Nano-carrier can be used to deliver drugs and are capable of controlled release for a continued period of time[39], which is advantageous for formulations requiring quick therapeutic effects as shown in Figure 11.

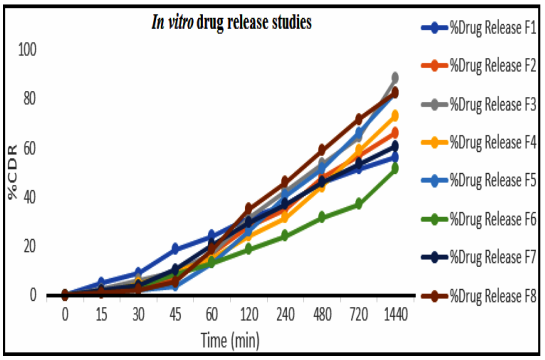

Fig. 11. Percentage drug release of roflumilast loaded NLCs

Table 3: PDI, Particle size, zeta potential, %Entrapment efficiency, %CDR various formulations of NLCs

Formulation	Particle size (nm) (Y1)	%EE(Y2)	%CDR(Y3)	PDI	Zeta Potential
F1	127.43	79.22	56.11	0.437	-9.9
F2	124.98	78.64	66.13	0.713	-14.79
F3	122.65	87.76	88.28	0.278	-20.16
F4	212.76	61.66	73.23	0.462	-13.14
F5	162.97	54.92	82.53	0.552	-14.78
F6	207.97	70.67	51.55	0.908	-14.24
F7	141.06	86.75	60.66	0.281	-5.6
F8	145.54	60.66	82.53	0.482	-12.12

CONCLUSION

The study used Tween 80, oleic acid, and glyceryl monostearate (GMS) to create and optimize nanostructured lipid carriers (NLCs) for the conveyance of Roflumilast. The optimized formulation (F3) demonstrated good stability and uniformity with favorable polydispersity index, zeta potential, and particle size. With a cumulative drug release (%CDR) and high entrapment efficiency, the NLC system proved to be successful in encapsulating and releasing Roflumilast. The study's experimental design incorporated a response surface methodology and a two-factor, three-level

factorial approach. The results demonstrated the noteworthy contributions of oleic acid and GMS in affecting drug release patterns, particle size, and entrapment efficiency. Roflumilast was successfully incorporated into the lipid matrix without causing any notable chemical interactions or degradation, as validated by characterization procedures. Further confirmation of the optimized NLCs' spherical morphology and nanoscale uniformity, both necessary for improved bioavailability and targeted drug delivery, came from transmission electron microscopy (TEM). By resolving the drawbacks of traditional delivery methods, the -optimized NLCs provide a reliable and effective drug delivery platform for Roflumilast. To further evaluate the therapeutic advantages and safety profile of the optimized NLC formulation, future research should concentrate on *in vivo* evaluations.

ACKNOWLEDGMENT

The authors acknowledge the resources provided by Teerthanker Mahaveer College of Pharmacy at Teerthanker Mahaveer University in Moradabad, and Babasaheb Bhimrao Ambedkar University in Lucknow which allowed them to finish this study.

Conflicts of interest

The authors have reported no financial or additional potential conflicts with an interest in this research.

REFERENCES

1. Mehnert, W.; Mäder, K. Solid Lipid Nanoparticles: Production, Characterization and Applications., *Adv Drug Deliv Rev.*, **2012**, *64*, 83–101.
2. Fang, C.-L.; A Al-Suwayeh, S.; Fang, J.-Y. Nanostructured Lipid Carriers (NLCs) for Drug Delivery and Targeting., *Recent Pat Nanotechnol.,* **2013**, *7*(1), 41–55.
3. Fang, J.-Y.; Fang, C.-L.; Liu, C.-H.; Su, Y.-H. Lipid Nanoparticles as Vehicles for Topical Psoralen Delivery: Solid Lipid Nanoparticles (SLN) versus Nanostructured Lipid Carriers (NLC)., *European Journal of Pharmaceutics and Biopharmaceutics.*, **2008**, *70*(2), 633–640.
4. Wheeler, L. A.; Aswad, A.; Connor, M. J.; Lowe, N. Depletion of Cutaneous Glutathione and the Induction of Inflammation by 8-Methoxypsoralen plus UVA Radiation., *Journal of Investigative Dermatology.,* **1986**, *87*(5), 658–662.
5. Ruffilli, I.; Ragusa, F.; Benvenga, S.; Vita, R.; Antonelli, A.; Fallahi, P.; Ferrari, S. M. Psoriasis, Psoriatic Arthritis, and Thyroid Autoimmunity., *Front Endocrinol* (Lausanne)., **2017**, *8*, 139.
6. Schafer, P. Apremilast Mechanism of Action and Application to Psoriasis and Psoriatic Arthritis., *Biochem Pharmacol.,* **2012**, *83*(12), 1583–1590.
7. Card, G. L.; England, B. P.; Suzuki, Y.; Fong, D.; Powell, B.; Lee, B.; Luu, C.; Tabrizizad, M.; Gillette, S.; Ibrahim, P. N. Structural Basis for the Activity of Drugs That Inhibit Phosphodiesterases., *Structure.*, **2004**, *12*(12), 2233–2247.
8. Moustafa, F.; Feldman, S. R. A Review of Phosphodiesterase-Inhibition and the Potential Role for Phosphodiesterase 4-Inhibitors in Clinical Dermatology., *Dermatol Online J.*, **2014**, *20*(5).
9. Pincelli, C.; Schafer, P. H.; French, L. E.; Augustin, M.; Krueger, J. G. Mechanisms Underlying the Clinical Effects of Apremilast for Psoriasis., *J Drugs Dermatol.*, **2018**, *17*(8), 835–840.
10. Li, H.; Zuo, J.; Tang, W. Phosphodiesterase-4 Inhibitors for the Treatment of Inflammatory Diseases., *Front Pharmacol.*, **2018**, *9*, 409-585.
11. Administration, U. S. F. and D. OTEZLA ®(Apremilast) Prescribing Information., **2017**.
12. Lebwohl, M. G.; Papp, K. A.; Stein Gold, L.; Gooderham, M. J.; Kircik, L. H.; Draelos, Z. D.; Kempers, S. E.; Zirwas, M.; Smith, K.; Osborne, D. W. Trial of Roflumilast Cream for Chronic Plaque Psoriasis., *New England Journal of Medicine.*, **2020**, *383*(3), 229–239.
13. Schafer, P. H.; Parton, A.; Capone, L.; Cedzik, D.; Brady, H.; Evans, J. F.; Man, H.-W.; Muller, G. W.; Stirling, D. I.; Chopra, R. Apremilast Is a Selective PDE4 Inhibitor with Regulatory Effects on Innate Immunity., *Cell Signal.*, **2014**, *26*(9), 2016–2029.
14. Raveendra, B.; Kiran, S.; Kumari, V.; Jyothi, R.; Bhavani, D. UV Spectrophotometric Method for the Estimation of Roflumilast in Human Serum., *Pharmaceutica Analitica Acta.*, **2016**, *7*(6), 1–4.

15. Zhou, G.-P.; Troy, F. A. Characterization by NMR and Molecular Modeling of the Binding of Polyisoprenols and Polyisoprenyl Recognition Sequence Peptides: 3D Structure of the Complexes Reveals Sites of Specific Interactions., *Glycobiology*., **2003**, *13*(2), 51–71.
16. Ali, F.; Kumar, R.; Sahu, P. L.; Singh, G. N. Physicochemical Characterization and Compatibility Study of Roflumilast with Various Pharmaceutical Excipients., *J Therm Anal Calorim*., **2017**, *130*, 1627–1641.
17. Pardeike, J.; Weber, S.; Haber, T.; Wagner, J.; Zarfl, H. P.; Plank, H.; Zimmer, A. Development of an Itraconazole-Loaded Nanostructured Lipid Carrier (NLC) Formulation for Pulmonary Application., *Int J Pharm*., **2011**, *419*(1–2), 329–338.
18. Chauhan, M. K.; Sharma, P. K. Optimization and Characterization of Rivastigmine Nanolipid Carrier Loaded Transdermal Patches for the Treatment of Dementia., *Chem Phys Lipids*., **2019**, *224*, 104794.
19. Jahan, S.; Aqil, M.; Ahad, A.; Imam, S. S.; Waheed, A.; Qadir, A.; Ali, A. Nanostructured Lipid Carrier for Transdermal Gliclazide Delivery: Development and Optimization by Box-Behnken Design., *Inorganic and Nano-Metal Chemistry*., **2022**, 1–14.
20. Shah, J.; Nair, A. B.; Shah, H.; Jacob, S.; Shehata, T. M.; Morsy, M. A. Enhancement in Antinociceptive and Anti-Inflammatory Effects of Tramadol by Transdermal Proniosome Gel., *Asian J Pharm Sci*., **2020**, *15*(6), 786–796.
21. Suo, M.; Zhao, X.; Yu, G.; Zhang, W. Lidocaine Loaded Nanostructured Lipid Carriers for Prolonged Local Anesthesia: In Vitro and in Vivo Studies., *J Dispers Sci Technol*., **2022**, *43*(5), 682–689.
22. Patel, D.; Dasgupta, S.; Dey, S.; Ramani, Y. R.; Ray, S.; Mazumder, B. Nanostructured Lipid Carriers (NLC)-Based Gel for the Topical Delivery of Aceclofenac: Preparation, Characterization, and in vivo Evaluation., *Sci Pharm*., **2012**, *80*(3), 749.
23. Catauro, M.; Barrino, F.; Dal Poggetto, G.; Crescente, G.; Piccolella, S.; Pacifico, S. New SiO_2/Caffeic Acid Hybrid Materials: Synthesis, Spectroscopic Characterization, and Bioactivity., *Materials*., **2020**, *13*(2), 394.
24. Wang, J.-Z.; Yan, C.-H.; Zhang, X.-R.; Tu, Q.-B.; Xu, Y.; Sheng, S.; Wu, F.-A.; Wang, J. A Novel Nanoparticle Loaded with Methyl Caffeate and Caffeic Acid Phenethyl Ester against Ralstonia Solanacearum-a Plant Pathogenic Bacteria., *RSC Adv*., **2020**, *10*(7), 3978–3990.
25. Pinho, E.; Henriques, M.; Soares, G. Caffeic Acid Loading Wound Dressing: Physicochemical and Biological Characterization., *Ther Deliv*., **2014**, *5*(10), 1063–1075.
26. Shah, N. V; Seth, A. K.; Balaraman, R.; Aundhia, C. J.; Maheshwari, R. A.; Parmar, G. R. Nanostructured Lipid Carriers for Oral Bioavailability Enhancement of Raloxifene: Design and In vivo Study., *J Adv Res*., **2016**, *7*(3), 423–434.
27. Sharma, O. P.; Patel, V.; Mehta, T. Design of Experiment Approach in Development of Febuxostat Nanocrystal: Application of Soluplus® as Stabilizer., *Powder Technol.,* **2016**, *302*, 396–405.
28. Sinha, P.; Srivastava, S.; Mishra, N.; Singh, D. K.; Luqman, S.; Chanda, D.; Yadav, N. P. Development, Optimization, and Characterization of a Novel Tea Tree Oil Nanogel Using Response Surface Methodology., *Drug Dev Ind Pharm*., **2016**, *42*(9), 1434–1445.
29. Keshri, L.; Pathak, K. Development of Thermodynamically Stable Nanostructured Lipid Carrier System Using Central Composite Design for Zero Order Permeation of Econazole Nitrate through Epidermis., *Pharm Dev Technol*., **2013**, *18*(3), 634–644.
30. Bhatt, S.; Sharma, J. B.; Kamboj, R.; Kumar, M.; Saini, V.; Mandge, S. Design and Optimization of Febuxostat-Loaded Nano Lipid Carriers Using Full Factorial Design., *Turk J Pharm Sci*., **2021**, *18*(1), 61.
31. Bolton, S.; Bon, C., *Practical and Clinical Applications. Pharm Stat*., **2004**, 308–337.
32. Abbas, H.; Refai, H.; El Sayed, N. Superparamagnetic Iron Oxide–Loaded Lipid Nanocarriers Incorporated in Thermosensitive in Situ Gel for Magnetic Brain Targeting of Clonazepam., *J Pharm Sci*., **2018**, *107*(8), 2119–2127.

33. Müller, R. H.; Mäder, K.; Gohla, S. Solid Lipid Nanoparticles (SLN) for Controlled Drug Delivery–a Review of the State of the Art., *European Journal of Pharmaceutics and Biopharmaceutics*., **2000**, *50*(1), 161–177.
34. Kohli, A. K.; Alpar, H. O. Potential Use of Nanoparticles for Transcutaneous Vaccine Delivery: Effect of Particle Size and Charge., *Int J Pharm*., **2004**, *275*(1–2), 13–17.
35. Gonzalez-Mira, E.; Egea, M. A.; Garcia, M. L.; Souto, E. B. Design and Ocular Tolerance of Flurbiprofen Loaded Ultrasound-Engineered NLC., *Colloids Surf B Biointerfaces*., **2010**, *81*(2), 412–421.
36. Kamath, P. P.; Rajeevan, R.; Maity, S.; Nayak, Y.; Narayan, R.; Mehta, C. H.; Velagacherla, V.; Konuri, A.; Nayak, U. Y. Development of Nanostructured Lipid Carriers Loaded Caffeic Acid Topical Cream for Prevention of Inflammation in Wistar Rat Model., *J Appl Pharm Sci*., **2023**, *13*(1), 64–75.
37. Dikmen, G.; Guney, G.; Genc, L. Characterization of Solid Lipid Nanoparticles Containing Caffeic Acid and Determination of Its Effects on MCF-7 Cells., *Recent Pat Anticancer Drug Discov*., **2015**, *10*(2), 224–232.
38. Madane, R. G.; Mahajan, H. S. Curcumin-Loaded Nanostructured Lipid Carriers (NLCs) for Nasal Administration: Design, Characterization, and In vivo Study., *Drug Deliv.,* **2016**, *23*(4), 1326–1334.
39. Fattahi F, Khoddami A, Avinc O. Poly (lactic acid) nanofibres as drug delivery systems: Opportunities and challenges., *Nanomedicine Research Journal*., **2019,** *1;4*(3), 130-40.